Received: 8 January 2020 | Revised: 29 June 2020 | Accepted: 1 July 2020
DOI: 10.1002/eqe.3321

RESEARCH ARTICLE

WILEY

Experimental and numerical studies on buckling restrained braces with posttensioned carbon fiber composite cables

Kurtulus Atasever[1,2] | **Shogo Inanaga**[3] | **Toru Takeuchi**[3] | **Yuki Terazawa**[3] | **Oguz C. Celik**[4]

[1]Department of Architecture, Mimar Sinan Fine Arts University, Istanbul, Turkey
[2]Earthquake Engineering and Disaster Management Institute, Istanbul Technical University, Istanbul, Turkey
[3]Department of Architecture and Building Engineering, Tokyo Institute of Technology, Tokyo, Japan
[4]Department of Architecture, Istanbul Technical University, Istanbul, Turkey

Correspondence
Kurtulus Atasever, Department of Architecture, Mimar Sinan Fine Arts University, Istanbul, Turkey.
Email: kurtulus.atasever@msgsu.edu.tr

Funding information
TUBITAK 2214-A International Doctoral Research Fellowship Programme

Summary

There has been an increasing interest in using residual deformation as a seismic performance indicator for earthquake resistant building design. Self-centering braced structural systems are viable candidates for minimizing residual deformations following a major earthquake. Hence, this study proposes an alternative type of buckling restrained brace (BRB) with externally attached posttensioned (PT-BRB) carbon fiber composite cables (CFCCs). The steel core of the brace is used as an energy dissipator, whereas the CFCCs provide the self-centering force for minimizing residual story drifts. Three proof-of-concept specimens are designed, fabricated, and cyclically tested at different posttensioning force levels. The CFCC behavior to obtain cyclic response, including the anchorage system, is examined closely. A parametric study is also conducted to show the effect of the different configurations of PT-BRBs on the inelastic response. Furthermore, optimal brace parameters are discussed to realize design recommendations. The results indicated that the implementation of partially self-centering BRBs in building frames can lead to the target residual displacements. A stable behavior is obtained for the proposed PT-BRBs when subjected to the loading protocol specified in the American Institute of Steel Construction (AISC) 2016 Seismic Provisions.

KEYWORDS

buckling restrained brace, carbon fiber composite cable, partially self-centering, residual deformation, self-centering

1 | INTRODUCTION

Conventional seismic design practices and current codes allow buildings to experience large plastic deformations under a design basis earthquake (DBE).[1] The use of such code criteria results in significantly damaged buildings that do not return to their original positions, and large amount of residual displacements hinder the reuse of these buildings following a major earthquake. Hence, buildings are sacrificed after a major earthquake while safety of lives is assured. The loss of damaged buildings and reconstruction of new buildings significantly impacts the economy[2] and environment.[3]

Macrae and Kawashima[4] showed that residual deformations are mainly dependent on postyield stiffness ratio (α) for elasto-plastic hysteresis, and they decrease as α increases. Thus, one possible solution to minimize residual deformations, which is commonly used in the Japanese design practice, is the concept of damage controlled building.[5] This concept constitutes a dual system composed of moment resisting (MR) frames that support gravity loads and added seismic dampers for mainly resisting lateral loads. MR frames provide additional postyield stiffness to elasto-plastic dampers (such as metallic or friction dampers); thus, the MR frames aid in reducing residual deformations.

The residual deformations can also potentially be mitigated by self-centering (SC) structures. They have been proposed in various structural configurations such as frames incorporating posttensioned/pretensioned beam-to-column connections,[6,7] rocking frames,[8] or SC-braced frames.[9] SC behavior is generally realized by adding restoring forces to the structural system for recentering the building after an earthquake. Christopoulos et al.[10] investigated seismic response of SC single degree of freedom systems. They showed that no residual deformation and peak deformation similar to that of elasto-plastic behavior can be obtained when flag-shaped behavior is provided. Zhu and Zhang[11] developed an SC brace by using shape memory alloys (SMAs). However, the proposed brace exhibited relatively low damping values when compared with metallic or viscous dampers. Christopoulos et al.[12] developed and tested[13] an SC brace, which consists of a damper with friction-based energy dissipation mechanism and aramid base tendons. Chou and Chen[14] tested braces of similar concept with steel, e-glass fiber, and T-700 carbon fiber tendons. In addition to friction-based energy dissipation mechanisms, buckling restrained braces (BRBs) have been introduced in an SC brace.[15] BRBs exhibit an excellent energy dissipation capacity, and they have been used as seismic dampers in seismically vulnerable areas, such as Turkey, Japan, the United States, Taiwan, Canada, and New Zealand, since the first application of BRBs in 1988 by Fujimoto et al.[16] However, connection details/types of frames incorporated with BRB exhibit a significant impact on the overall behavior. For example, implementation of BRBs in buildings with a non-MR frame results in high residual displacements following a major earthquake.[17,18] Miller et al.[15] developed a self-centering BRB (SC-BRB), which consists of a mortar-filled BRB for energy dissipation and SMA rods for the SC mechanism. Specifically, SMAs are useful in seismic applications for the required recentering force and energy dissipation. However, they are expensive and difficult to process. Subsequently, the concept of SC-BRB was modified by Zhou et al.,[19] wherein an all-steel dual tube BRB is combined with basalt fiber reinforced polymer cables (BFRPCs). They reported that prestress loss and elastic modulus of BFRPC increases under cyclic loading.

This study extends the concept of SC-BRBs by describing an alternative type of posttensioned buckling restrained brace (PT-BRB). The proposed PT-BRB is expected to be used as a full or partial SC-BRB or a BRB with high postyield stiffness ratio, which behaves similar to dual systems without requiring an MR beam to column connection detail. The PT-BRB consists of mortar-filled BRB for energy dissipation and posttensioned carbon fiber composite cables (CFCCs) for the SC mechanism. A more simplified brace design is proposed here, when compared with previously developed SC-BRB, by using an inner tube for restraining the buckling of the core and for transferring restoring forces in the SC mechanism. CFCCs exhibit linear and easily predictable behavior when compared with SMAs. Their elastic modulus is similar to that of steel strands and exhibit higher corrosion resistance and elastic elongation capacity. The CFCCs are used for the first time in SC-BRBs proposed in this study. Hence, special emphasis is placed on coupon tests of CFCCs and the effect of anchorage system, which plays a significant role on the overall brace performance. Three proof-of-concept BRB specimens were designed and tested in a diagonal brace configuration under varying levels of posttensioning (PT) forces in the cables. Additionally, a thorough parametric numerical study was conducted to show the impact of PT-BRBs on steel-framed buildings. Full SC hysteresis decreases the energy-dissipating performance of the braces when compared with that of a conventional bilinear hysteresis. Therefore, a trade-off relationship exists between the reduction in maximum response and residual drift. An optimal combination of SC force and postyield stiffness are discussed to control maximum response and residual drift.

2 | CONCEPT AND PRELIMINARY DESIGN OF THE PT-BRBS

Conventional BRBs can be combined with symmetrically placed four posttensioned CFCCs to develop a brace with SC (complete or partial) capabilities. PT-BRBs consist of a steel core, an inner tube (it), an outer tube (ot), two end plates, and four CFCCs. Specifically, the use of CFCCs in providing the required PT for the brace is novel idea. Figure 1A shows the production steps of the proposed PT-BRBs. First, a steel core is produced and welded to the core stiffeners (step 1). Second, the core is placed into an inner tube wherein only left-side of the tube is welded to the core stiffeners and mortar is filled into the inner tube (step 2). Once the production of the energy dissipating element of the brace (i.e., BRB) is completed, it is placed inside the outer tube, and only right-side of tube is welded to the core stiffeners (step 3). Finally, CFCCs and end plates are placed in the brace without any welding, and a PT force is applied to the CFCCs (step 4). The production process of the BRB is very similar to that of a conventional BRB with the exception of the welding of the inner tube. This type of welding aids in the use of the inner tube as a casing tube of the BRB and as

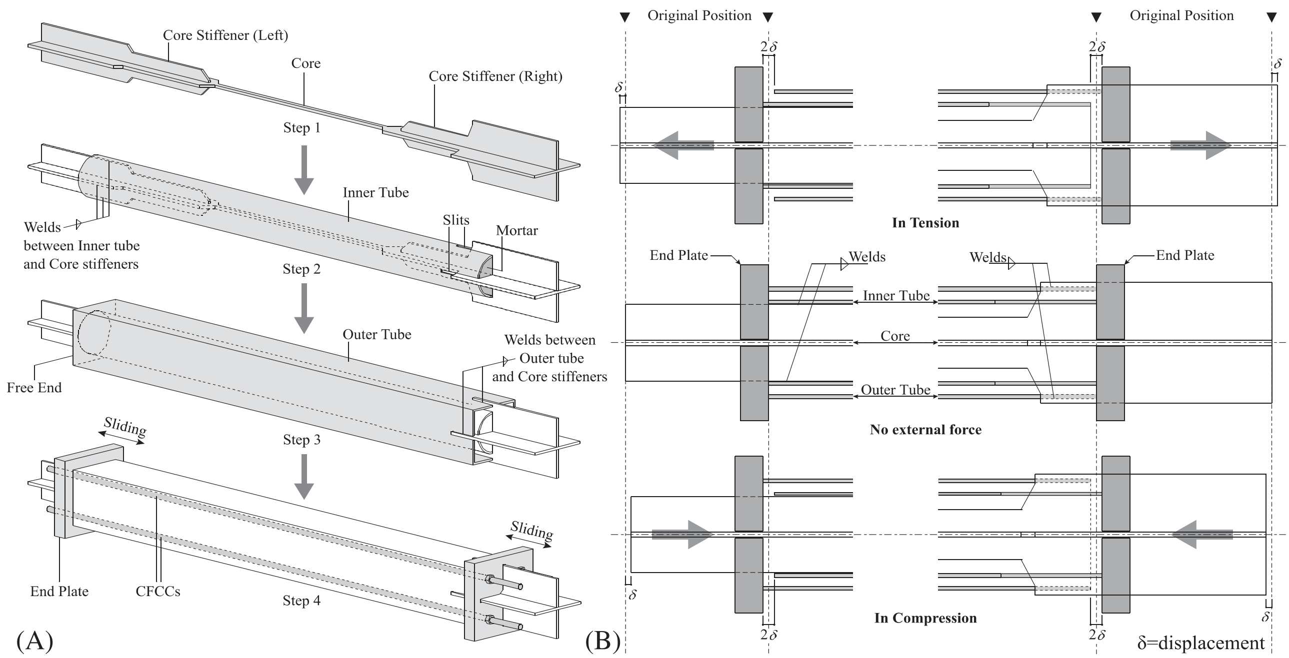

FIGURE 1 Posttensioned buckling restrained brace (PT-BRB) A, production steps and B, gap opening mechanism

an element for the SC mechanism. The main purpose of the SC mechanism is to change the direction of the compression force by 180°, thereby transferring it to the cables. This is realized by creating a gap for tension and compression cases (Figure 1B) to maintain tension in CFCCs. In the case of no force, tubes touch the end plates because of the PT force in the cables. When the brace moves under tension, welded parts of the tubes push the end plates, and thus, a gap is created between the end plates and free parts of the tubes. In compression, a part of the forces on the brace is transferred through the tubes to the end plates. Hence, gaps are created between the end plates and welded parts of the tubes.

Previous studies have demonstrated that residual deformations are mainly dependent on postyield stiffness ratio (α) and energy dissipation ratio (β) for bilinear and flag-shaped hysteresis.[4,10,20] Therefore, α and β values of the braces are selected as two major parameters in designing any type of PT-BRBs. The first stiffness of posttensioned systems is generally not clear or lower than the calculated values.[21,22] Hence, in this study, α is adopted as a ratio of postyield stiffness of the brace (K_2) to the first effective stiffness ($K_{1\text{-}eff}$), as shown in Equation 1, where $F_{y\text{-}B}$ denotes the axial force on the brace at the yield displacement of the brace ($\delta_{y\text{-}B}$) and BRB ($\delta_{y\text{-}BRB}$).

$$K_{1-eff} = \frac{F_{y-B}}{\delta_{y-B}}. \tag{1}$$

The preliminary design of PT-BRBs is based on two assumptions: SC-mechanisms exhibit multilinear elastic behavior (Figure 2A), and BRBs exhibit an elastic-perfectly plastic behavior (Figure 2B). Thus, $F_{y\text{-}B}$ (Equation 2) can be

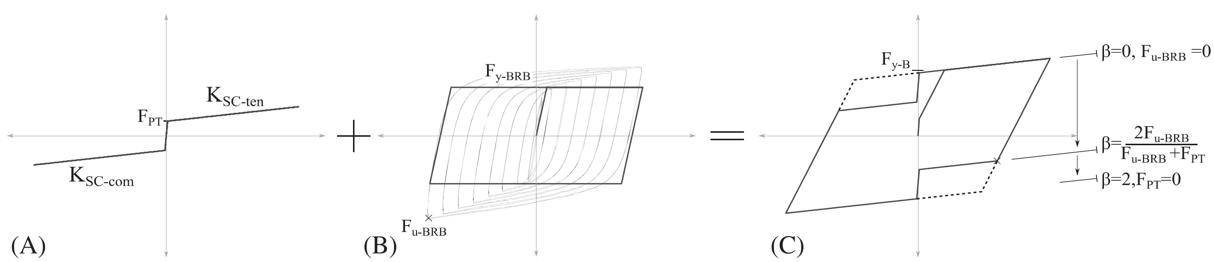

FIGURE 2 Design concept of posttensioned buckling restrained brace (PT-BRB) A, self-centering (SC) mechanism, B, BRB, and C, total behaviors

estimated with sum of the SC mechanism and BRB model (Figure 2C) by assuming that the posttension force (F_{PT}) is transferred instantly. In Equation 2, $F_{y\text{-}BRB}$ and $K_{SC\text{-}ten}$ denote yield force of the BRB and the equivalent stiffness of the SC mechanism in tension, respectively.

$$F_{y-B} = F_{y-BRB} + F_{PT} + \delta_{y-BRB} K_{SC-ten}. \tag{2}$$

The energy dissipation ratio parameter (β) in Equation 3 denotes the SC capability of the brace (Figure 2). This is demonstrated by the fact that when PT force (F_{PT}) is equal to the ultimate strength of the BRB ($F_{u\text{-}BRB}$), β becomes unity. This implies that the brace has sufficient force to recenter after the earthquake has lasted. Furthermore, $\beta = 2$ implies that PT-BRB is a conventional BRB and when $1 < \beta < 2$, the brace becomes a partial SC-BRB.

$$\beta = \frac{2 \cdot F_{u-BRB}}{F_{u-BRB} + F_{PT}}. \tag{3}$$

The strain hardening adjustment factor (ω) of the core and compression strength adjustment factor of the BRB ($\beta_{co\text{-}BRB}$) increase $F_{u\text{-}BRB}$ (Equation 4). Hence, the elastic-perfectly plastic BRB model assumption is not used in the calculation of β.

$$F_{u-BRB} = \beta_{co-BRB} \omega F_{y-BRB}. \tag{4}$$

The tubes are inactive in tension. Hence, the equivalent stiffness of the SC mechanism in tension ($K_{SC\text{-}ten}$) (Equation 5) is equal to total stiffness of the (n) CFCCs, which is slightly different than that in compression ($K_{SC\text{-}com}$) (Equation 6). Hence, there is a difference in the equivalent stiffness of the brace in compression ($K_{B\text{-}com}$) (Equation 7) and tension ($K_{B\text{-}ten}$) (Equation 8). Subscripts for equivalent stiffnesses (K) denote the corresponding names of the components, such as core regions E1, E2, E3, E4, E5, and E6 in Figure 3.

$$K_{SC-ten} = n \cdot K_{CFCC}, \tag{5}$$

$$K_{SC-com} = \left(\frac{1}{K_{it}} + \frac{1}{K_{ot}} + \frac{1}{n \cdot K_{CFCC}} \right)^{-1}, \tag{6}$$

$$K_{B-com} = \left(\frac{1}{K_{BRB} + K_{SC-com}} + \frac{1}{K_{E1}} + \frac{1}{K_{E6}} \right)^{-1}, \tag{7}$$

$$K_{B-ten} = \left(\frac{1}{K_{BRB} + n \cdot K_{CFCC}} + \frac{1}{K_{E1}} + \frac{1}{K_{E6}} \right)^{-1}. \tag{8}$$

The equivalent stiffness of the BRB (K_{BRB}) is calculated as per Equation 9 where α_{BRB} is the postyield stiffness ratio of the BRB and is assumed as 0.02.[23]

$$K_{BRB} = \left(\frac{1}{\alpha_{BRB} \cdot K_{core}} + \frac{1}{K_{E2}} + \frac{1}{K_{E3}} + \frac{1}{K_{E4}} + \frac{1}{K_{E5}} \right)^{-1}. \tag{9}$$

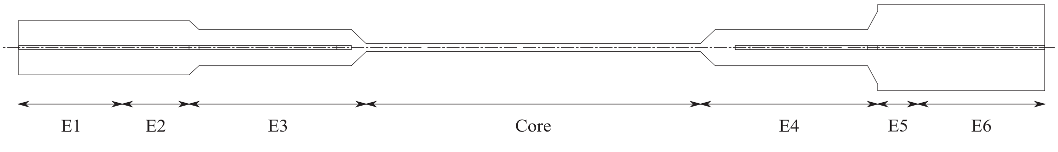

FIGURE 3 Regions for calculating equivalent stiffnesses

The size, shape, materials, yield (σ_y) or ultimate (σ_u) strength, elastic modulus (E), cross-section area (A), length (L), and stiffness (K) of the corresponding regions used in the production of the PT-BRB are listed in Table 1.

Three identical specimens, with the exception of the PT levels, are designed and produced for the experiments in the study. The capacity of the hydraulic actuator (500 kN) used in the experiment is the main limitation in the design of the specimens, and this is common in many experimental studies. Hence, the minimum possible core cross-section (12 × 25 mm) was designed to ensure that the maximum possible PT force can be applied without exceeding the hydraulic actuator's capacity. In the next step, locally available CFCC cables were selected and PT-BRB-80 was designed. Specimen PT-BRB-80 was designed to ensure minimum possible β values (maximum PT force) by considering the actuator force capacity, minimum required elongation, and uncertainty in prediction of material and geometric properties such as yield stress, cable stiffness, and hardening parameters. PT-BRB-56 (partially SC-BRB) and PT-BRB-16 (bilinear BRB) were obtained by reducing the provided PT. PT-BRB-16 is designed such that it is similar to a conventional BRB but with relatively high postyield stiffness. PT forces on PT-BRB-16, PT-BRB-56, and PT-BRB-80 are approximately 5%, 18%, and 26% of the breaking load of the cables, respectively. The last two characters in the name of the brace denote value of the PT force in kN. In the design of PT-BRB, two main objectives were considered: (1) to investigate the impact of PT force on the characteristics of the brace and (2) to check whether the elongation capacity of the brace is suitable for the current codes. A minimum story drift ratio of $\Delta = 2\%$ (also proposed for life safety [LS] performance level in many seismic codes e.g., ASCE/SEI 7-16[24]) is considered for the experimental protocols developed in this study. The compression strength adjustment factor of the BRB ($\beta_{co\text{-}BRB}$) and strain hardening adjustment factor (ω) are assumed to be higher than the typical values[25] when the ultimate force of the brace ($F_{u\text{-}B}$) is calculated. The parameters calculated before the production of PT-BRBs are presented in Table 2 where T+, C−, and Δ represent tension, compression, and story drift ratio, respectively. As mentioned earlier, actuator force capacity was the major limitation in selecting the parameters α and β for the experiments of this study. However, in the design of a building, α can be freely selected when β is selected as 2.0 (i.e., bilinear systems). Partial and full SC systems, where β can be freely selected and α is be merely dependent on β, are discussed in the numerical part of the paper.

TABLE 1 Characteristics of PT-BRBs

Region	Shape	Size (mm)	Material	σ_y (MPa)	E (GPa)	n	A (mm²)	L (mm)	K (kN/mm)
Core	▌	12 × 25	SN400B	235–355	205	-	300	1000	61.5
E1	✚	171 × 171 × 12					3960	310	2618.7
E2		171 × 171 × 12					3960	200	4059.0
E3		113 × 112 × 12					2556	530	988.6
E4		113 × 112 × 12					2556	530	988.6
E5		270 × 270 × 12					6336	120	10 824.0
E6		270 × 270 × 12					6336	380	3148.1
Inner tube (it)	○	190.7 × 8.2	STK 490	315			4701	2380	404.9
Outer tube (ot)	□	250 × 250 × 9	BCR 295	295			8467	2380	729.3
CFCCs		7.5	CFCC	2444 (σ_u)	155	4	31.1	2350	8.2

Abbreviations: CFCCs, carbon fiber composite cables; PT-BRBs, posttensioned buckling restrained braces.

TABLE 2 Preliminary design values for the braces

Brace name	$F_{y\text{-}B}$ (kN)	$\delta_{y\text{-}B}$ (mm)	$K_{1\text{-}eff}$ (kN/mm)	K_2 (kN/mm) T+	K_2 (kN/mm) C−	α T+ (%)	α C− (%)	β	$F_{u\text{-}B}$ at $\Delta = \pm 2\%$ (kN) T+	$F_{u\text{-}B}$ at $\Delta = \pm 2\%$ (kN) C−	$\beta_{co\text{-}BRB}$	ω
PT-BRB-16	116.5	1.73	67.15	8.7	8.4	12.9	12.5	1.83	391.5	412.6	1.2	1.6
PT-BRB-56	156.2	1.76	88.74	8.7	8.4	9.8	9.5	1.50	431.0	452.1		
PT-BRB-80	180.0	1.78	101.39	8.7	8.4	8.5	8.3	1.35	454.7	475.8		

Abbreviation: PT-BRB, posttensioned buckling restrained brace.

3 | CYCLIC TESTING OF PT-BRBS

3.1 | Cyclic coupon tests for CFCCs

CFCCs are widely used in bridge constructions or as prestressing reinforcement elements in concrete elements.[26] Although their monotonic behavior is reported in detail by Kimura et al.,[27,28] there is a paucity of studies on the cyclic behavior of externally attached CFCC. To provide a better understanding of the behavior and performance of such cables under cyclic axial loads (not fully reversed to prevent buckling), CFCCs were placed in a universal testing machine (UTM) between the grips prior to the tests of the BRB specimens. Additionally, nuts were attached to the end of the steel sleeves to avoid possible slippage, which is a common problem in such tests. Free length of CFCC (L_f = 380 mm) specimens with approximately 50 times the diameter and a loading speed of 3.75 mm/min were deemed sufficient as per ASTM-D7205/D7205M.[29] The anchorage system with a highly expansive material (HEM) is used for fixing the CFCCs to the steel sleeves (Figure 4A). HEM expands because of the chemical reaction and creates high pressure between the steel sleeve and CFCC. This pressure without stress concentration provides an appropriate force transfer between the CFCC and steel sleeve.[30] The axial displacement was measured with two linear variable differential transformers (LVDT) for obtaining the cyclic behavior of CFCC including the anchorage performance. Similar to the study done by Bruce and Eatherton,[31] loading protocols (LPs) were adopted from FEMA 461.[32] Among the test coupons, CFCC-0 was not applied with any initial tension force, whereas CFCC-11.4 and CFCC-19 were tensioned to 15% and 25% of the design load, respectively. All the protocols were continued for a minimum of 10 steps (i.e., 20 cycles), and the next step amplitude was defined as a_{i+1}, which is 40% higher than the previous amplitude (Figure 4B). As shown in Figure 4C–E, cyclic responses of CFCC coupons are not linear. There are mainly two different stiffnesses wherein the first stiffness ($K_{CC\text{-}1}$) includes slippage or placing of the provided anchorage system. After permanent slippage, stiffness of CFCC increases and a linear behavior is observed for the second stiffness ($K_{CC\text{-}2}$), especially for CFCC-11.4 and CFCC-19. Specifically, CFCC-0 is not applied with any PT force. Hence, the stiffness decreases and becomes zero when the force on the cable is very low.

All specimens are tested such that they exhibit the guaranteed breaking load (P_g). Although some slippage occurred in CFCC-11.4, there was no visible damage or no stiffness degradation was observed after slippage. It is important to note that the average of the total strains (ε_t) and minimum linear elastic elongations (ε_e) were 4.83% and 2.07%, respectively. Linear elastic elongation (ε_e) of a CFCC is calculated in Equation 10 where P_{ult} and L_f denote the fracture force and free length of CFCC coupons, respectively. The total strain (ε_t) is calculated by dividing the elongation at the fracture to L_f. The results of the coupon tests of CFCCs, which reveal the ultimate strength (σ_u) and properties of the coupons, such as effective cross section area (A_{eff}) and elastic modulus (E) calculated from $K_{CC\text{-}2}$, are provided in Table 3.

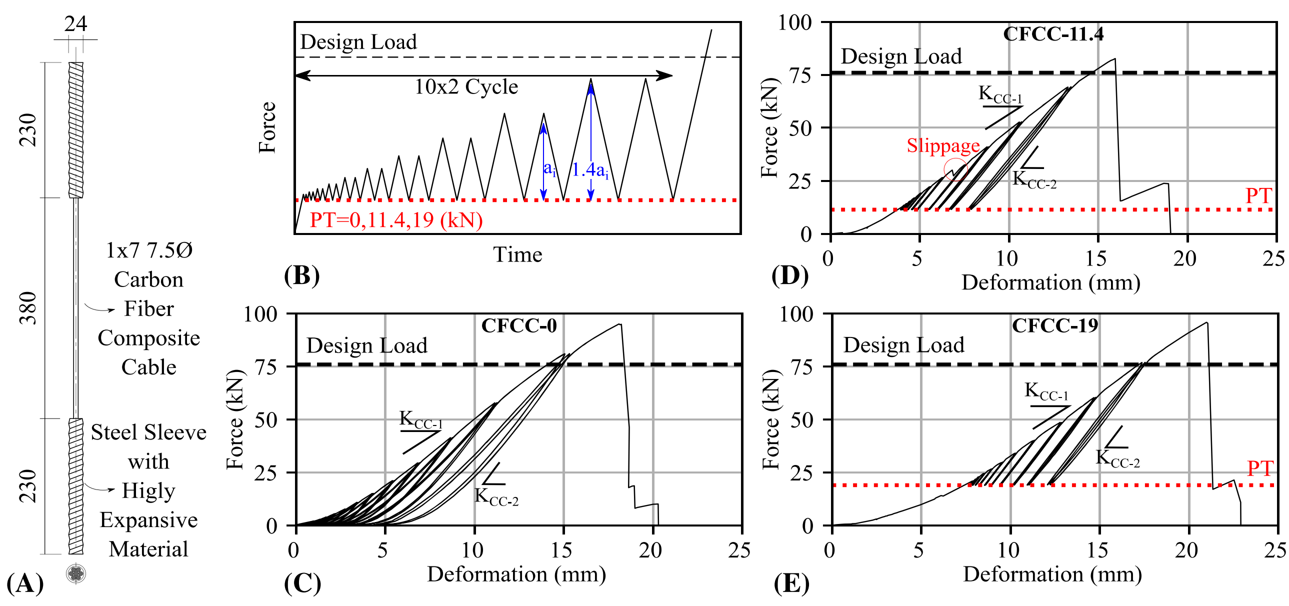

FIGURE 4 Coupon tests of carbon fiber composite cable (CFCC) A, CFCC geometry B, loading protocol, hysteretic curves of C, CFCC-0, D, CFCC-11.4, and E, CFCC-19 [Colour figure can be viewed at wileyonlinelibrary.com]

TABLE 3 Results of the CFCC coupon tests

Coupon 1×7 7.5 Ø	F_{PT} (kN)	L_f (mm)	A_{eff} (mm^2)	P_g (kN)	P_{ult} (kN)	σ_u (MPa)	$K_{CC\text{-}1}$ (kN/mm)	$K_{CC\text{-}2}$ (kN/mm)	E (GPa)	ε_t (%)	ε_e (%)
CFCC-0	0	380	31.1	76	95.11	3058	6.20	9.20	112.41	4.76	2.72
CFCC-11.4	11.4				82.68	2659	6.08	10.51	128.42	4.20	2.07
CFCC-19	19				95.86	3082	5.80	10.90	133.18	5.52	2.31
Average					91.22	2933	6.03	10.20	124.67	4.83	2.37

Abbreviation: CFCC, carbon fiber composite cable.

$$\varepsilon_e = \frac{P_{ult}}{K_{CC-2} L_f}. \tag{10}$$

When the CFCC specimen exceeds its ultimate deformation, the strength decreases drastically. It should be noted that all the wires did not fracture instantly. The experiment was continued until all the wires were fractured, and the images before (Figure 5A) and after (Figure 5B) fracture show brittle failure of CFCC. There was no damage at the anchorage system for any specimen (Figure 5C). Based on the results of the coupon tests, the following PT process was established. Each cable was pretensioned to 70 kN (around 92% of design strength of CFCC) and then released until the target PT force was realized. This eliminated permanent deformation of the anchorage system due to placing or slippage. Another advantage of this process ensured verification of the cable strength and stiffness before the BRB testing. The PT path is necessary to ensure a linear response because the CFCC is used as an external element to minimize residual deformations.

3.2 | Monotonic coupon tests of the steel core

SN400B type steel is used as the core element of the produced BRBs. From the four monotonically performed coupon tests, the average yield strain, fracture strain, tensile strength, and elastic modulus values were 0.13%, 33%, 283.81 MPa, 439.52 MPa, and 217.8 GPa, respectively.

3.3 | Test setup and loading protocol

PT-BRBs are placed diagonally into the test frame (Figure 6A). The angle between the loading direction and PT-BRB is $\theta = 25.34°$, which represents a typical configuration for diagonal braces attached to buildings with approximately 9-m beam spans. A displacement controlled testing was performed via a 500-kN capacity hydraulic actuator. All tests were conducted in the laboratory in the Ookayama Campus of Tokyo Institute of Technology (Midorigaoka Building 2). Both ends of the braces used pinned connection details, and one of them was attached to the posttensioned reaction beam to ensure a minimum gap between the reaction beam and frame during the experiment. Pin-to-pin and core lengths of the PT-BRBs are 3540 and 1000 mm, respectively. During the tests, displacements were measured via 12 displacement transducers. Reaction forces on CFCCs were significant, and thus they were recorded by four load cells. Additionally,

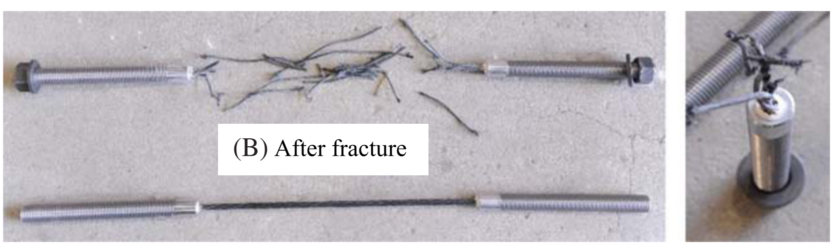

(A) Before fracture

(C) Anchorage after fracture

FIGURE 5 Images from carbon fiber composite cable (CFCC) coupon tests A, before fracture, B, after fracture, and C, anchorage after fracture [Colour figure can be viewed at wileyonlinelibrary.com]

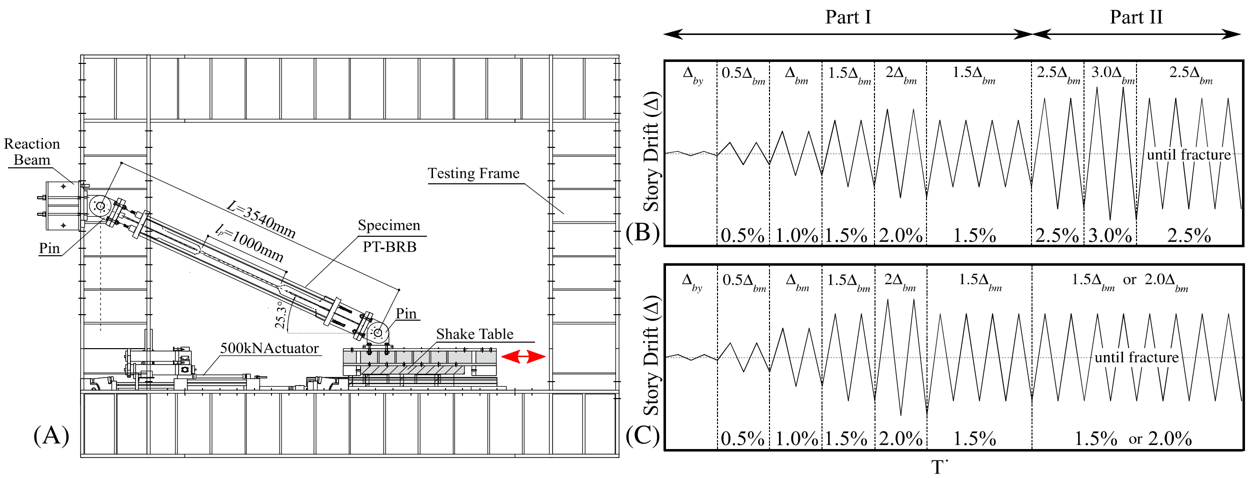

FIGURE 6 Schematic of specimens and displacement histories A, test setup, loading protocol of B, posttensioned buckling restrained brace (PT-BRB)-16, C, PT-BRB-56, and PT-BRB-80 [Colour figure can be viewed at wileyonlinelibrary.com]

strain gages were attached to the inner and outer tubes of the braces for monitoring the changes in force during the experiment.

In the first part of the LP, the American Institute of Steel Construction (AISC) protocol, which is a cyclic test for qualification of BRBs in ANSI/AISC 341-16,[33] was applied to all the specimens for a better comparison. The AISC protocol requires completion of two cycles of loading at the deformation corresponding to Δ_y, $0.5\Delta_{bm}$, $1.0\Delta_{bm}$, $1.5\Delta_{bm}$, and $2.0\Delta_{bm}$, where Δ_{bm} denotes design story drift and Δ_y denotes drift where the brace is yielded. Considering the elongation capacities of partial SC PT-BRBs (the elongation capacity of bilinear PT-BRB is higher), design story drift is limited to $\Delta_{bm} = 1\%$ as per ANSI/AISC 341-16.[33] This is similar to limiting the story drift ratios to 1% under the DBE and 2% under the maximum considered earthquake (MCE). The limit of the design story drift to 1% is quite common in Japan.[23] However, this limit is generally used for essential facilities (e.g., hospitals) in the United States.[24] Additional complete loading cycles at the deformation corresponding to $1.5\Delta_{bm}$ is required for the brace to realize cumulative inelastic axial deformation of at least 200 times the yield deformation. Due to relatively short core configuration of BRBs, PT-BRBs reached the required cumulative inelastic axial deformation even before the loading of the peak displacement level ($2.0\Delta_{bm}$) of the AISC protocol was reached. To compete with the conventional low cycle fatigue performance of BRB, the first part of LP (LP—part I) defined in this paper consists of the AISC protocol and four cycles of loading at the deformation corresponding to $1.5\Delta_{bm}$ even exceeds the required minimum cumulative inelastic deformation capacity (Figure 6B,C). In the second part of loading (LP—part II), all specimens were tested with different protocols. LPs of PT-BRB-56 and PT-BRB-80 (Figure 6C) were continued with a constant amplitude (1.5% and 2.0% story drifts, respectively) until fracture to determine low cycle fatigue performance of the core at different strain levels. As stated before, PT-BRB-16 was designed as a conventional BRB with high postyield stiffness. Hence, this BRB is expected to exhibit a higher elongation capacity because of the low PT force. Therefore, the LP of PT-BRB-16 (Figure 6B) was continued with increasing amplitudes of 2.5% and story drift ratios of 3.0% at every two cycles to verify higher elongation capacity of the brace. Another aim of the LPs was to determine the behavior of the brace after a component had failed (CFCC or BRB core). Therefore, LPs of PT-BRB-56 and PT-BRB-80 were continued even after the core fractured to observe the overall failure mode. Additionally, once the second part of protocol of PT-BRB-16 was completed, the CFCCs were released from PT-BRB-16. In this case, the hysteretic behavior of only the BRB was obtained, and thereby the sole response of the brace was observed for a scenario when the cables failed.

4 | TEST RESULTS

Images of the BRBs before the experiment and that of all braces and PT-BRB-16 in the test frame are shown in Figure 7. The properties of the braces, such as stiffness, yield force ($F_{y\text{-}B}$), yield displacement ($\delta_{y\text{-}B}$), peak force ($F_{u\text{-}B}$) at $\Delta = \pm 2\%$ drift, and compression strength adjustment factor ($\beta_{co\text{-}B}$), obtained via experimental tests are presented in Table 4. It is shown that $F_{y\text{-}B}$ and $K_{1\text{-}eff}$ increase with increasing levels of PT, as expected. Although the second

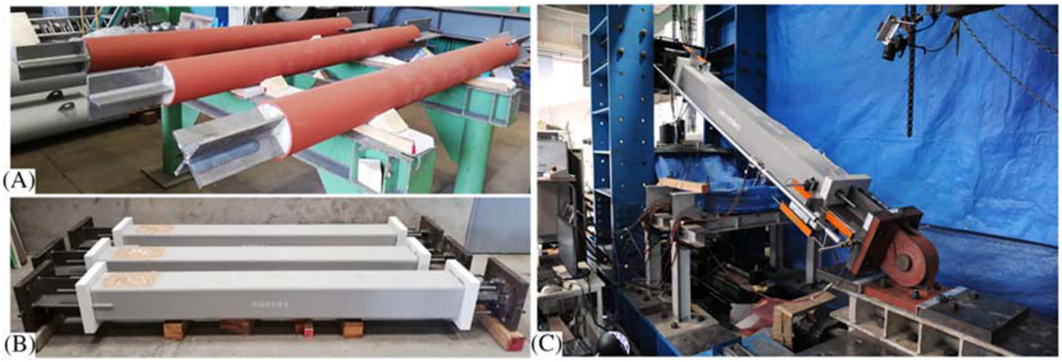

FIGURE 7 Images before experiment A, buckling restrained brace (BRBs) only, B, posttensioned buckling restrained braces (PT-BRBs), and C, PT-BRB-16 in the test frame [Colour figure can be viewed at wileyonlinelibrary.com]

TABLE 4 Brace properties from experimental data

				K_2 (kN/mm)		α			$F_{u\text{-}B}$ at $\Delta = \pm 2\%$ (kN)		
Brace name	$F_{y\text{-}B}$ (kN)	$\delta_{y\text{-}B}$ (mm)	$K_{1\text{-}eff}$ (kN/mm)	T+	C−	T+ (%)	C− (%)	β	T+	C−	$\beta_{co\text{-}B}$
PT-BRB-16	119.4	1.9	65.0	7.7	8.5	11.9	13.1	1.93	344.2	−372.4	1.08
PT-BRB-56	150.9	2.1	74.1	7.8	9.0	10.6	12.1	1.59	388.2	−456.8	1.18
PT-BRB-80	183.4	1.7	106.5	8.6	9.4	8.1	8.8	1.35	427.5	−455.3	1.07

Abbreviation: PT-BRB, posttensioned buckling restrained brace.

stiffnesses (K_2) of the braces are similar, α is the lowest for PT-BRB-80 mainly due to a higher $K_{1\text{-}eff}$. All the postyield stiffness ratios are higher than that of conventional BRBs.[23] Due to the compression overstrength, stiffness values after the BRBs yielded were slightly higher in the compression (C−) zone than in the tension zone (T+). The highest ratio of the maximum compression force to the maximum tension force ($\beta_{co\text{-}B}$) was 1.18 for PT-BRB-56, and this value was much lower than the allowable limit (1.5) as per ANSI/AISC 341-16. Energy dissipation ratio parameters (β) presented in this table are calculated at two times the design drift ($\Delta = 2\%$) level.

Cyclic responses of PT-BRBs are presented in three parts: (a) first part LP (LP—part I), (b) low cycle fatigue loading or increasing load protocol part (LP—part II), and (c) response after fracture of the BRB cores or release of CFCCs. Hysteretic curves obtained from the reversed cyclic testing of the developed PT-BRBs are presented in Figure 8. The AISC protocol was successfully completed for 1% design and 2% peak story drift levels without any premature failure, strength, or stiffness degradation.

Figure 8 reveals that PT-BRB-16 exhibits bilinear behavior, whereas PT-BRB-56 and PT-BRB-80 exhibit partially SC behaviors as per the design. These curves prove that the SC mechanism of the braces functioned correctly. Conversely, an SC mechanism does not instantly transfer forces as in an ideal condition. This phenomenon is emphasized and will be discussed later in this paper.

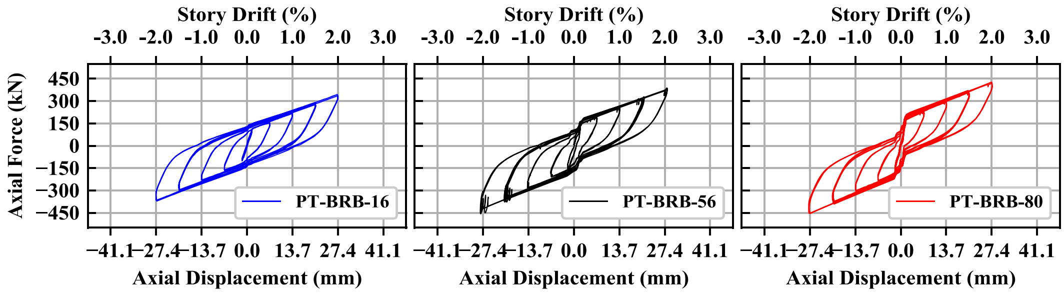

FIGURE 8 Hystereses of posttensioned buckling restrained braces (PT-BRBs) (loading protocol [LP]—part I) [Colour figure can be viewed at wileyonlinelibrary.com]

During the tests, an example of gap opening behavior is shown in Figure 9 for PT-BRB-80. When the brace is in compression, inner tube (red circular tube) pushes the lower end plate and a visible gap opens in the lower part of the brace (Figure 9A). In tension, the welded part of the inner tube pulls the upper end plate, and a visible gap opens in the upper part of the brace (Figure 9B).

After the first part of the LP was completed, low-cycle fatigue performance of PT-BRB-56 and PT-BRB-80 was investigated. Additionally, an increasing load was applied to PT-BRB-16 to determine the elongation capacity (Figure 10).

Furthermore, PT-BRB-56 completed 34 cycles at around 1.8% core strain before fracture, whereas PT-BRB-80 completed 13 cycles at around 2.5% core strain. PT-BRB-16 realized a 3.8% core strain, which is relatively high for current engineering practices.

At the last part of the LP, the failure modes of PT-BRBs are investigated (Figure 11). The first failure mode and the fracture of the core due to low-cycle fatigue were investigated for PT-BRB-56 and PT-BRB-80. The idea of testing the PT-BRB-16 at the last part of the LP involved investigating the failure modes of the cables. Given that the cables did not

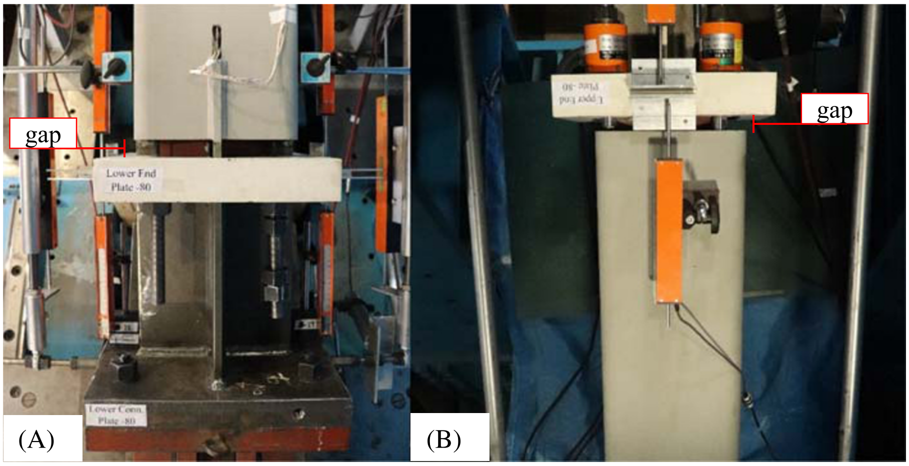

FIGURE 9 Posttensioned buckling restrained brace (PT-BRB)-80 gap opening at A, $-2\Delta_{bm}$ and B, $+2\Delta_{bm}$ [Colour figure can be viewed at wileyonlinelibrary.com]

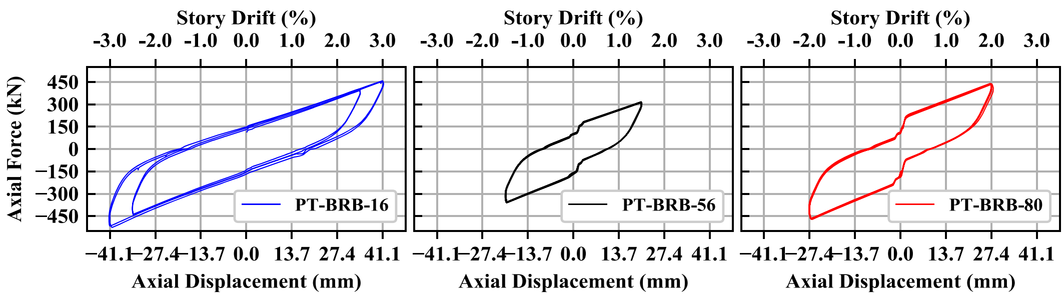

FIGURE 10 Hystereses of posttensioned buckling restrained braces (PT-BRBs) (loading protocol [LP]—part II) [Colour figure can be viewed at wileyonlinelibrary.com]

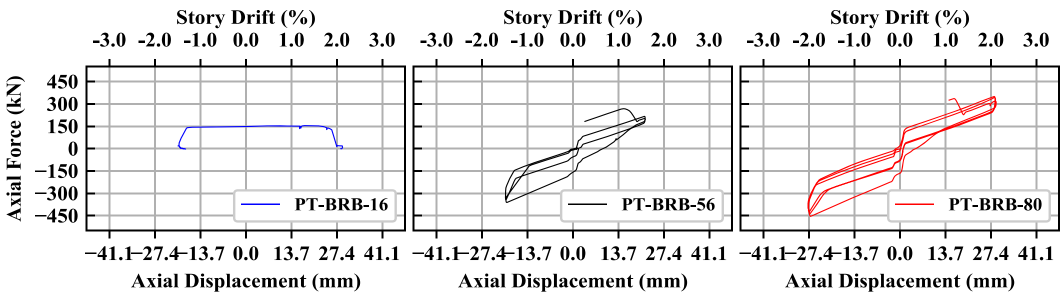

FIGURE 11 Hystereses of posttensioned buckling restrained braces (PT-BRBs) (loading after failure of core or release of carbon fiber composite cables [CFCCs]) [Colour figure can be viewed at wileyonlinelibrary.com]

fail during the experiment, they were released and only bare BRB was planned to be tested. However, before completing one cycle, the BRB failed due to the low cycle fatigue of the core. This was also expected because a core strain of approximately 3.8% was observed until this stage. Hence, it can be seen that braces are stable without a core or any PT cables (Figure 11).

The sum of the responses of CFCCs are given for the first part of the LP in Figure 12A. Owing to the PT force path of PT-BRBs, there were no permanent deformations due to the end anchorage system. The attached cables exhibited linear behavior without any significant changes in the stiffness.

CFCC-80 and CFCC-56 exhibited very stable and constant cyclic response under low cycle fatigue load (Figure 12B). There was a drop in force reaction of CFCC-16 at +1.25% story drift. This reduction in force occurred instantly due to the relaxation of the cables on the upper side of end plates. This behavior could potentially be due to the rotation of end plates. The end plates touch core stiffeners due its rotation and create an interaction between the end plate and core stiffeners. This causes an instant release of force on the cables when it reaches a certain force limit. The effect of this drop in force on the hystereses is observed to be limited and temporary. The cables showed stable response even after the core fractured (Figure 12C). Behavioral values of CFCCs of PT-BRBs from cyclic tests are shown in Table 5. Loss of posttension is a crucial issue in SC systems and is limited for partially SC braces (especially when PT is high). Cables of PT-BRB-80 are slightly stiffer than other cables. Elastic modulus values of cables used in PT-BRBs (Table 5) are approximately 20% higher than CFCC coupon tests values (Table 3). The difference may be due to different boundary conditions and loading path applied to CFCCs for PT-BRBs. Elastic strain (ε_e) is calculated as the sum of the strain from initial PT force and strain due to peak deformation during cyclic loading. A 1.75% of total elastic strain (ε_e) is obtained at a peak force of 314.3 kN for CFCC-16.

Cumulative plastic deformation parameter (CPD) can be defined as the ratio of cumulative plastic deformation to the yield deformation. This is calculated for the core (CPD_{core}) and brace (CPD_B) itself. The CPD_{core} is calculated by using the gap deformation that consists of elastic deformation of the restrainers inside the tubes although the elastic deformation is expected to be very low. The CPD_B is calculated by using axial plastic deformation of the brace as defined in ANSI/AISC 341-16.[33] The CPD values and number of cycles related to the core strain are listed in Table 6. Increases in the peak strain decreases the low cycle fatigue (or fracture) life of the brace. However, cumulative deformation capacity of the brace (PT-BRB-16) with the lowest CPD_B is approximately 3.7 times the cumulative plastic deformation required to achieve the AISC protocol ($CPD_{AISC} = 200$).

Equivalent viscous damping (ζ_{eqv}) values are significant while evaluating the seismic effectiveness of the developed BRBs. The values are calculated for all PT-BRBs and presented in Figure 13A. They generally reach peak values in

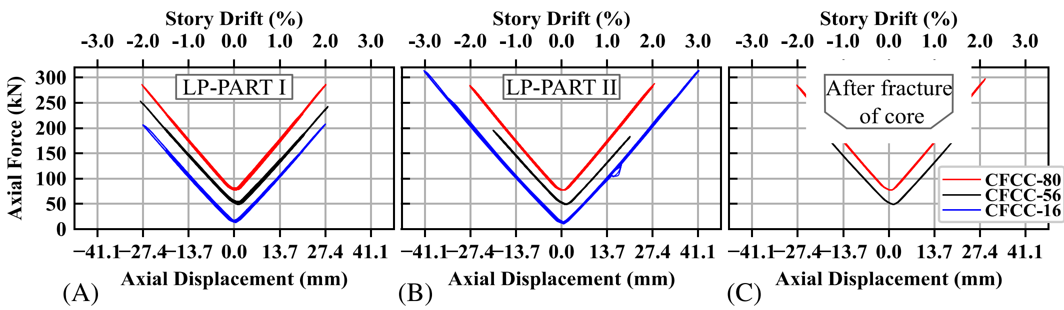

FIGURE 12 Hystereses of carbon fiber composite cables (CFCCs) for A, loading protocol (LP)—part I, B, LP—part II, and C, loading after failure of core [Colour figure can be viewed at wileyonlinelibrary.com]

TABLE 5 Behavioral values of CFCCs of PT-BRBs

	L_f	Initial F_{PT}	PT loss (%)	PT loss (kN)	$4 \times K_{CFCC}$ (kN/mm)	E (GPa)	Peak disp. (mm)	Peak strain (%)	PT strain (%)	ε_e (%)	P_{ult} (kN)
CFCC-16	2350	16.34	42	6.81	7.77	146.70	39.0	1.66	0.09	1.75	314.3
CFCC-56		56.07	13	7.44	7.72	145.76	26.4	1.12	0.31	1.43	253.5
CFCC-80		80.43	4	3.38	8.22	155.22	26.7	1.14	0.42	1.55	297.4

Abbreviations: CFCC, carbon fiber composite cable; PT-BRBs, posttensioned buckling restrained braces.

TABLE 6 Number of cycles and fatigue characteristics

	Core strain	0.0%	0.5%	1.2%	1.8%	2.5%	3.1%	3.8%	CPD_{core}	CPD_B
PT-BRB-16	Number of cycles	2	2	2	6	2	2	2	951	734
PT-BRB-56		2	2	2	34	2	-	-	1893	1342
PT-BRB-80		2	2	2	6	13	-	-	1421	1137

Abbreviations: CPD, cumulative plastic deformation; PT-BRB, posttensioned buckling restrained brace.

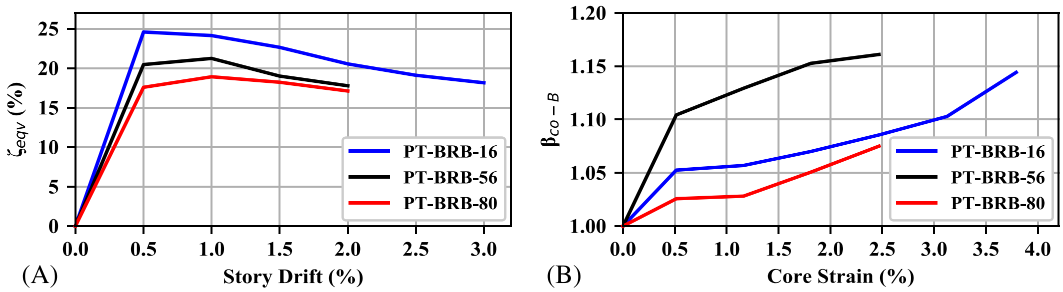

FIGURE 13 Comparing specimens A, equivalent viscous damping ratio and B, compression strength adjustment factor [Colour figure can be viewed at wileyonlinelibrary.com]

between 0.5% and 1% story drifts and slightly decrease until the termination of testing. The minimum value of ζ_{eqv} exceeds 17% for all specimens. Average compression strength adjustment factor ($\beta_{co\text{-}B}$) of all cycles at each displacement levels is shown in Figure 13B. Effect of repeated cycle number or amount of PT force on $\beta_{co\text{-}B}$ is not observed during the experiments. However, increases in core strains increase $\beta_{co\text{-}B.}$

4.1 | Load transfer within the transition zone

Recentering force mechanism is expected to be active when the brace returns to its original position where displacement is zero. Theoretically, the force transfer should be instant when the tubes touch the end plates. However, it is observed that the force transfer occurs smoothly with more than one step. Figure 14A shows the hysteretic behavior of PT-BRB-80 with response from inner and outer tubes for the first part of protocol. Forces at the inner and outer tubes are calculated by using data obtained from the strain gauges. Strain gauges' data are corrected with available load cell data. Responses of each cable are shown in Figure 14B for the same LP. To better understand the restoring force mechanism, Figure 14C presents a zoomed in view of Figure 14A,B and is divided into five regions. The force transfer steps in these regions may be classified as follows:

Region I: When the brace returns from the tension to compression zone, end tubes initially touch the outer tube. In this region, forces on the inner tube are very low, and most of the cable force is resisted by the outer tube because the outer tube is slightly longer than the inner tube.

Region II: In this region, most of the forces on the cables are carried by the outer tube, whereas the brace force is governed by the BRB.

Region III: A part of the inner tube touches the end plate, and thus, force is transferred to the inner tube. In the end of the region, CFCC-1 and CFCC-4 complete the transfer of the load to the inner tube.

Region IV: In this region, CFCC-1 and CFCC-4 start to elongate although CFCC-2 and CFCC-3 do not affect brace behavior. Second stiffness of the brace is governed by CFCC-1 and CFCC-4.

Region V: Force transfer from CFCC-2 and CFCC-3 to the inner tube is completed in this region. Transition of axial force from tension to compression (or vice versa) is completed within a ±2 mm displacement level. There are mainly two reasons for the mechanism: tube length tolerance and rotation of the brace parts (end plates, tubes, core, and restrainers). Rotation of the brace is also observed in both directions when loading is in the transition zone. Given this behavior, the force transfer mechanism lasts for multiple steps and is smoothly in contrast to the theoretical assumptions adopted in the study.

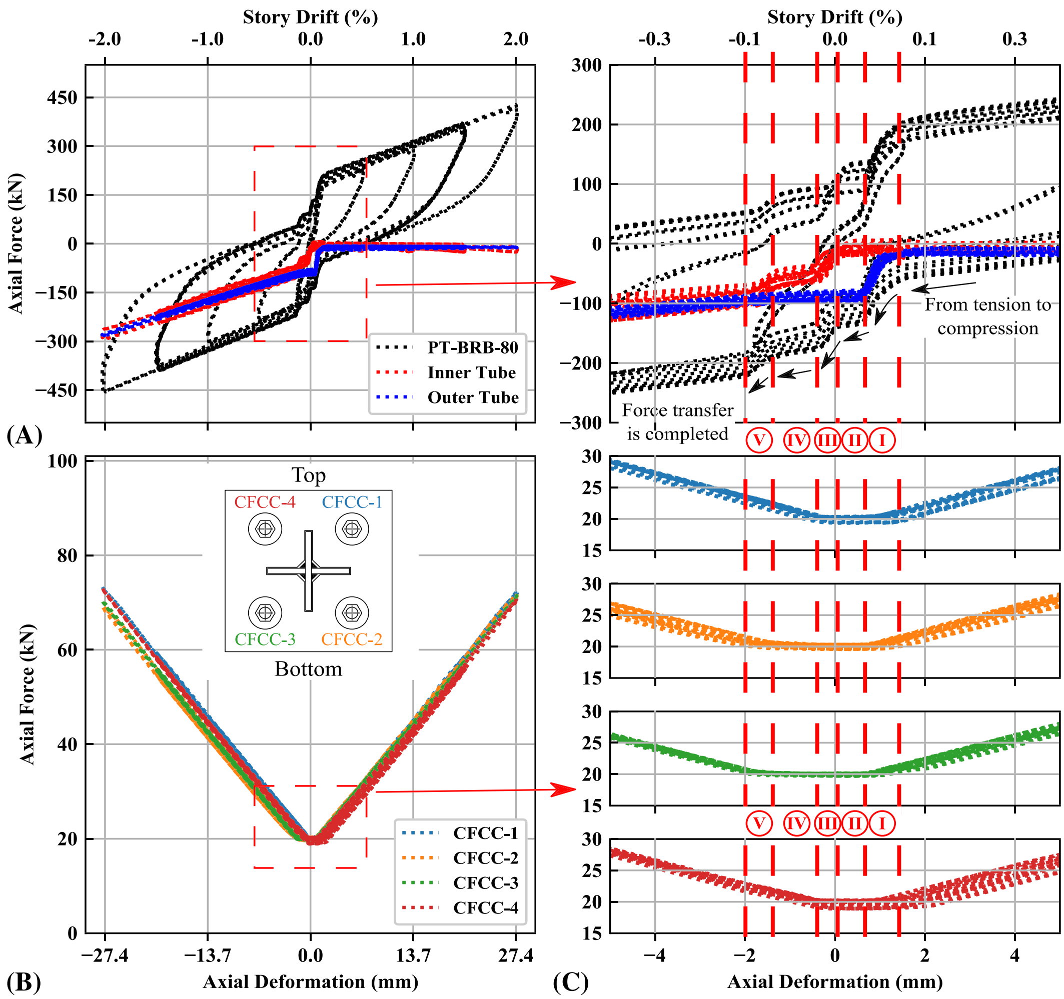

FIGURE 14 Restoring force mechanism of posttensioned buckling restrained brace (PT-BRB)-80 A, overall and tube hystereses, B, carbon fiber composite cables (CFCCs) hystereses, C, zoomed versions of corresponding figures [Colour figure can be viewed at wileyonlinelibrary.com]

5 | NUMERICAL ANALYSES

Numerical analyses were performed by OpenSeesPy with the Python programming language interpreter[34] of OpenSees (the Open System for Earthquake Engineering Simulation). Component and system modeling issues are discussed here. Component modeling is considered as a verification, whereas the system modeling is performed to show the effect of design parameters of PT-BRBs on the overall behavior of a building frame.

5.1 | Component modeling

The brace is modeled (Figure 15A) based on an earlier study by Eatherton et al.[35] The core is assumed as a force-based fiber element, whereas cables and tubes are treated as truss elements. Elastic beam-column element is assigned to end connections (i.e., regions C1 and C4) of the brace and transition parts (i.e., regions C2 and C3) of the BRB. Gap opening behavior is simulated by using multipoint constraints and zero length elements. Core material is modeled as SteelMPF, which is an extended Menegetto-Pinto model[36] to avoid inaccurate partial stress increase after partial unloading in the cyclic or dynamic analyses.[37] Yield strength (σ_y = 317.87 MPa), initial tangent modulus (E_0 = 217.8 GPa), strain hardening ratios (bp = 0.003 and bn = 0.018,), initial value of the curvature parameter (R0 = 15), curvature degradation parameters (cR1 = 0.8, cR2 = 0.0015), and isotropic hardening parameters (a1 = 0.024, a2 = 1, a3 = 0.020, and a4 = 1)

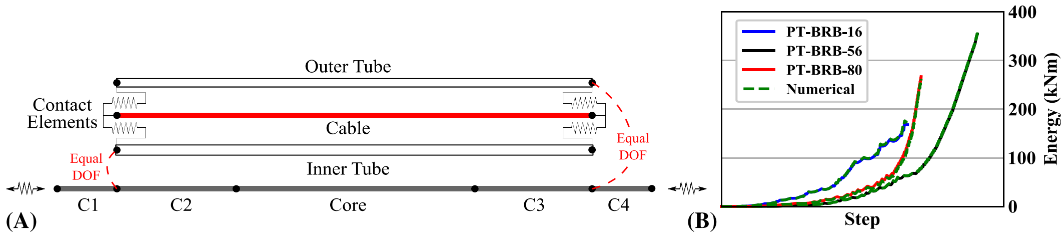

FIGURE 15 Modeling of posttensioned buckling restrained brace (PT-BRB) and dissipated energies A, brace model with names of component parts B, comparison between numerical and experimental cumulative energy until fracture [Colour figure can be viewed at wileyonlinelibrary.com]

are parameters that are required to create the SteelMPF model. Dissipated energies and obtained hysteretic curves are shown in Figures 15B and 16, respectively, and belong to experimental and numerical studies before fracture and are in very good agreement. The component model easily captures stiffness after yielding and peak forces. Although initial stiffness of numerical model slightly exceeds that in the actual case, it does not significantly affect the overall dynamic behavior of the brace.[21]

5.2 | System modeling: example building

The geometry and seismic weight of the selected building (Figure 17A) is adopted from FEMA P695.[38] The building which is a typical six-story office building in the United States has 9.00 × 9.00 m spans for the main frames. Story heights are 4.00 m for the ground story and 3.5 m for the rest of the building. It is assumed that bare frames of the building have "simple beam-to-column connections" which have negligible MR capacity. Therefore, the bare frames may be designed only for the gravity loads and for capacity-based design forces coming from the braces. Dead and live loads are assigned as 5 kN/m^2, 2.4 kN/m^2 for floors and 4 kN/m^2, 1 kN/m^2 for the roof, respectively. Because 100% of the lateral forces will be resisted by the braces (i.e., PT-BRBs), beams and columns of the structure are assumed as mainly elastic with required rotation capacities. All beam sections are W21X62, and column sizes are given in Figure 17A. The brace angle is similar to that in the experimental study. Selected bracing configuration is a two-story X-bracing configuration in which it is expected to minimize axial loads from unbalanced brace forces to the frame elements. Given the change in stiffness of yielding elements,[39] a 2% of Rayleigh damping is assigned to only the elastic part of structures at 0.2 and 2.0 times of the first periods. Column bases and beam-to-column connections are assumed as perfectly pinned. The brace model is similar to the component model and is repeated for each story.

Equivalent lateral load procedure[24] with a response modification factor of $R = 6$ is used to determine the design base shear forces. Several extant studies focus on the factor R for buckling restrained braced frames (BRBFs), thereby revealing that the factor R is generally in the range of 3.5 to 8 (e.g., Sabelli et al. and Bosco and Marino[17,40]). Additionally, it is noted that different seismic design provisions allow the use of different response modification factors in design (e.g., $R = 4.8$ for Canada, $R = 8$ for the United States, and $R = 4.3$ for New Zealand[41]). Conservatively, an acceptable value for R factor of 6 is assigned. The building importance factor of $I = 1.5$ is used to limit design story drift of 1% for

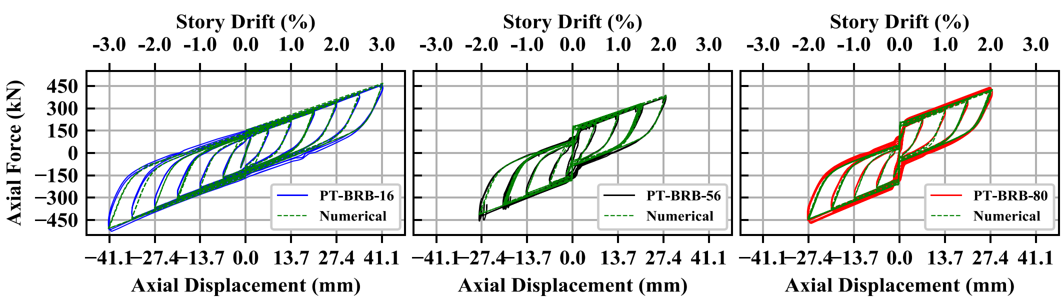

FIGURE 16 Comparison between numerical and experimental hystereses until fracture [Colour figure can be viewed at wileyonlinelibrary.com]

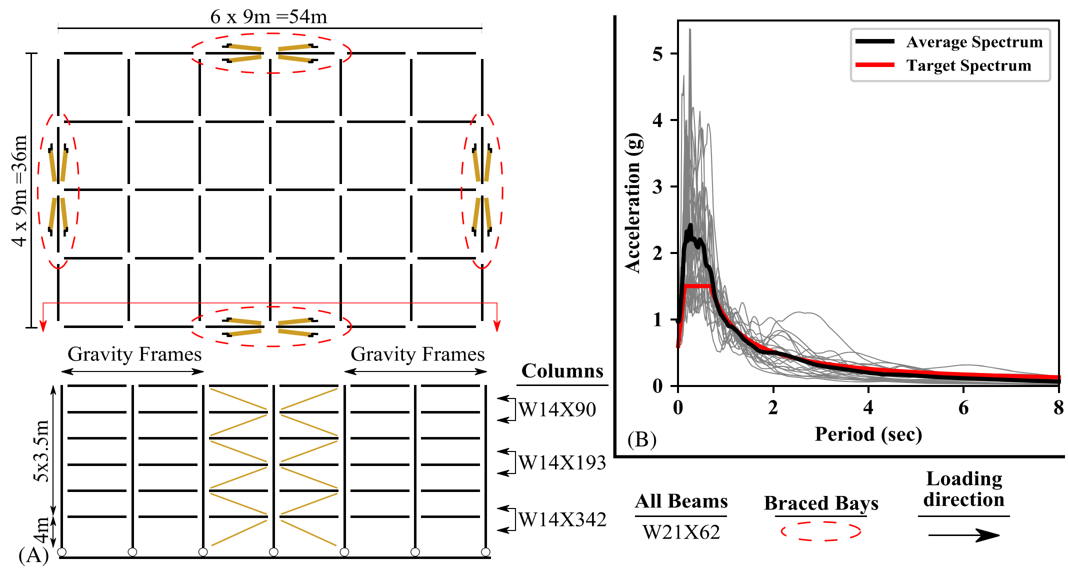

FIGURE 17 Example building and acceleration spectrum curves A, plan and elevation of building, B, scaled response spectrum [Colour figure can be viewed at wileyonlinelibrary.com]

the DBE level and 2% for the MCE level. These are compatible with the experimental results obtained in the study. Response history analyses are performed under MCE level to check story drifts. Target MCE spectra are calculated by assuming the structure in San Francisco area on a stiff soil. The mapped DBE spectral response acceleration parameters are $S_d = 1.0$, $S_{d1} = 0.68$, and $t_l = 12$. Far field ground motions dataset is adopted from FEMA P695 study, and 22 ground motion records are scaled to the target spectra via minimizing mean squared error[42] between 0.2 and 2 s periods (Figure 17B). Names and record sequence number (RSN)[43] of ground motions selected for the time-history analyses and their scale factors are given in Table 7.

The braces are designed by using an energy dissipation ratio parameter (β) such that they are consistent with extant studies.[10,20] A parametric study is conducted from fully SC brace ($\beta = 1$) to the conventional BRB ($\beta = 2$) (i.e., for β values of 1.00, 1.10, 1.20, 1.30, 1.40, 1.50, 1.60, 1.70, 1.80, 1.90, 1.92, 1.94, 1.96, 1.98, and 2.00). Based on the current design practice, $F_{y\text{-}B}$ is maintained as the same for all versions of brace design to compare seismic responses fairly. When the length (L), elastic modulus (E), and ultimate strength (σ_u) of the modeled brace parts (Figure 15) are expressed as ratios of core characteristics, Equation 11 is expressed as

$$R_{L-CFCC} = \frac{L_{CFCC}}{L_{core}}, R_{L-C1,4} = \frac{L_{C1,4}}{L_{core}}, R_{L-C2,3} = \frac{L_{C2,3}}{L_{core}}, R_E = \frac{E_{CFCC}}{E_{core}}, R_S = \frac{\sigma_{u-CFCC}}{\sigma_{y-core}}. \tag{11}$$

Given the limited elongation capacity of cables, the amount of PT stress is limited to $R_{PT} = 15\%$ of ultimate strength of the cable material ($\sigma_{u\text{-}CFCC}$). A safety factor of $s_f = 1/0.75$ (ANSI/AISC 360-16) is used when designing the tubes and connection parts of the brace to keep them elastic against compression. Capacity design forces or expected ultimate forces (F_u) on the interior connections (i.e., regions C2 and C3), tubes, and end connections (i.e., regions C1 and C4) or brace ($F_{u\text{-}B}$) are calculated by Equations 12 to 14, respectively.

$$F_{u-C2,3} = F_{u-BRB} s_f, \tag{12}$$

$$F_{u-tubes} = F_{u-CFCC} s_f, \tag{13}$$

$$F_{u-B} = F_{u-C1,4} = (F_{u-BRB} + F_{u-CFCC}) s_f, \tag{14}$$

If the same material is used for all steel parts of the brace, then the core area (A_{core}) of PT-BRBs is obtained from Equation 2 as in Equation 15.

TABLE 7 Selected ground motions and scale factors

RSN	Earthquake name	Year	Station name	H1 component name	H1 scale factor DBE	H1 scale factor MCE	H2 component name	H2 scale factor DBE	H2 scale factor MCE
68	San Fernando	1971	LA—Hollywood Stor FF	PEL090	2.81	4.21	PEL180	4.86	7.29
125	Friuli Italy-01	1976	Tolmezzo	A-TMZ000	2.76	4.15	A-TMZ270	2.53	3.79
169	Imperial Valley-06	1979	Delta	H-DLT262	2.12	3.18	H-DLT352	1.47	2.21
174	Imperial Valley-06	1979	El Centro Array #11	H-E11140	1.72	2.58	H-E11230	2.04	3.06
721	Superstition Hills-02	1987	El Centro Imp. Co. Cent	B-ICC000	1.61	2.42	B-ICC090	1.97	2.96
725	Superstition Hills-02	1987	Poe road (temp)	B-POE270	1.88	2.81	B-POE360	2.10	3.15
848	Landers	1992	Cool water	CLW-LN	2.57	3.86	CLW-TR	1.42	2.13
960	Northridge-01	1994	Canyon Country—W Lost Cany	LOS000	1.39	2.09	LOS270	1.31	1.97
1116	Kobe Japan	1995	Shin-Osaka	SHI000	1.96	2.94	SHI090	1.94	2.91
5780	Iwate Japan	2008	Iwadeyama	54015NS	2.20	3.29	54015EW	1.57	2.36
6890	Darfield New Zealand	2010	Christchurch Cashmere High School	CMHSN10E	1.70	2.55	CMHSS80E	2.93	4.40

Abbreviations: DBE, design basis earthquake; MCE, maximum considered earthquake; RSN, record sequence number.

$$A_{core} = \frac{F_{y-B}}{\sigma_{y-BRB}\left(\frac{h(2-\beta)}{\beta} + \frac{R_E\left(2R_{L-con2,3} + s_f h\right)(2-\beta)}{R_{L-CFCC}R_{PT}R_S\beta s_f} + 1\right)}. \tag{15}$$

Design forces of $F_{y\text{-}B}$ are increased with 1.3 redundancy factor for calculation of A_{core} as defined in ASCE.[24] Geometry of the brace is selected as a ratio of work point-to-work point length (L_B). Core length, end connections, and cables are assumed as 40%, 10%, and 80% of L_B, respectively. In the brace model, tubes and cables are assumed to exhibit the same length. Elastic strain (ε_e) of cables is limited to 1.58% to generalize the brace model although minimum elastic strain from coupon test results exceeded the value. The E_{CFCC} corresponds to 155 GPa. Multiplication of compressive ($\beta_{co\text{-}BRB}$) and strain hardening (ω) parameters is assumed as $h = 1.32$, which is consistent with the experimental study that focus on BRBs.[44]

Ratio of ultimate design force of SC brace to ultimate design force of brace when $\beta = 2$ is shown in Figure 18A. The graph shows the manner in which the over-strength force for design increases when SC force increases. Note that due to minor effect of gravity frames on lateral behavior of the building, beam and column sizes were maintained as

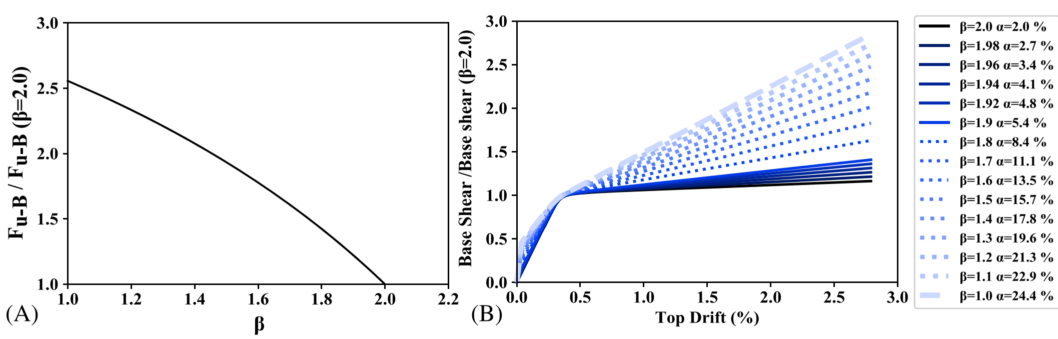

FIGURE 18 Representation of ultimate design forces A, relation between β and design force of connection elements of posttensioned buckling restrained braces (PT-BRBs), B, pushover curves for six-story steel frame with PT-BRBs [Colour figure can be viewed at wileyonlinelibrary.com]

identical for different β values. The required steel core areas of PT-BRBs are obtained as being between 13.3 and 163.2 cm^2. The maximum cable area is 62.2 cm^2.

A pushover analysis is also performed to obtain a better representation of the effect of β parameters on the overall system behavior. A displacement-controlled loading pattern is applied to the building following the same shape of the first mode. Given the initial prestress assumption, first stiffness of the SC braces increases when β values decrease (Figure 18B). In the experimental part of the study, three identical specimens exhibit a similar second stiffness, and this is mainly from the same total cable area used. Therefore, increases in PT force (i.e., decreasing β) increases $F_{y\text{-}B}$ and $K_{1\text{-}eff}$, whereas K_2 is constant because α decreases. However, as shown in Figure 18B, $F_{y\text{-}B}$ and $K_{1\text{-}eff}$ values are very similar to each other as designed. Decreases in β increase the cable area to keep the elongation capacity at the same level with other β configurations and again increases K_2 and α. It should be noted that trend of α in the experiments and numerical part is different because the goal of the experimental research differs from the building design perspective.

For each braced system with various β and α values that cover a wide range of structural properties, average peak and residual drift ratios obtained for selected 22 ground motions are shown in Figure 19. It is observed that increases in PT force (for lower values of β) increases peak drifts in upper stories and decreases residual drifts. Residual deformations of the conventional BRBs ($\beta = 2.0$) are highest (as expected) among other PT force levels and exceed 0.5% perceivable limit defined by McCormick et al.[45] When β equals 1.8 or is lower and given α values of 8.4% or higher, the building incorporating PT-BRBs displays optimal performance by experiencing negligible residual deformations.

Decrease in β to 1.9 also decreases peak drifts. However, in case when β is less than 1.5, there are significant drifts in upper stories, which exceed the common code limit of 2%. Standard deviations of peak and residual drifts are calculated to show dispersion of individual ground motion results. The results indicate that sum of average peak drift ratios and corresponding standard deviations are less than 3.5% for all cases. Sum of average residual drift ratios and corresponding standard deviations are less than 0.13% for $\beta \leq 1.8$ and reach 1.54% for conventional BRBs ($\beta = 2.0$).

The RSN1116 Kobe and RSN960 Northridge-01 ground motion records are used, and nonlinear time history analysis results are also presented to determine individual PT-BRB responses. The obtained hysteretic curves are shown in Figure 20 for different β values and braces at first, third, and roof stories. In order to enable a better comparison, axial force (F) on brace is normalized to design brace force ($F_{B\text{-}Story}$) of each story. Deformation of the conventional BRB ($\beta = 2.0$) concentrates at between 0.5% and 1.5% story drifts given the absence of the restoring force. Thus, a brace with low postyield stiffness does not return to the original position when the earthquake loading lasts and may result in significant residual drifts. It should be noted that although story drifts in the case of fully SC system ($\beta = 1.0$) concentrate around its origin position, high postyield stiffness increases the reaction force such that it exceeds twice $F_{y\text{-}B}$ and especially at the roof story. The cases in between two extremes (i.e., $\beta = 1.0$ and $\beta = 2.0$), such as when $\beta = 1.5$ or $\beta = 1.8$, can be termed as "partially self-centering braces". The partially SC PT-BRBs pose very small amount of residual deformations, thereby revealing that neither fully SC nor classical BRBs are optimal alternatives when considering all behavioral values for braced steel frames. This is an important outcome of the numerical part of the study. Additionally, the ultimate force of brace when $\beta = 1.8$, is lower than the case in $\beta = 1.5$. Average dissipated energies (cumulative area under hysteretic curves) of the braces for $\beta = 1.0$ are approximately 32% and 40% less than the case when $\beta = 2.0$ for ground motion records Kobe-H1 and Northridge-H1 respectively. However, the dissipated energy for $\beta = 1.8$ is very similar to that of conventional BRBs.

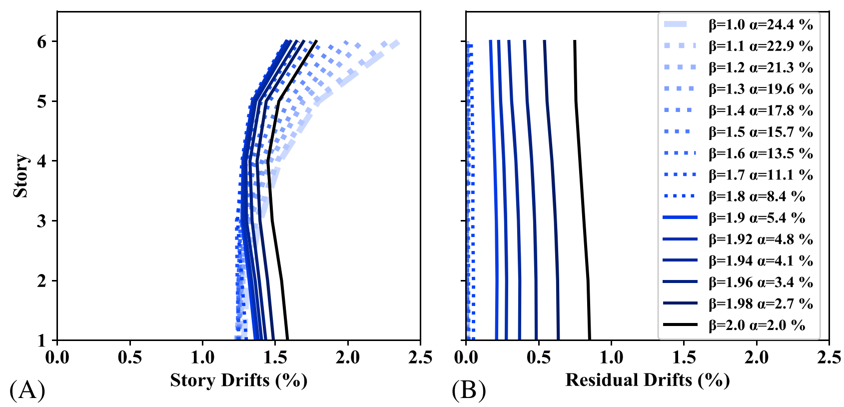

FIGURE 19 Calculated drift values A, average peak and B, residual drift ratios for six-story steel frame with posttensioned buckling restrained braces (PT-BRBs) [Colour figure can be viewed at wileyonlinelibrary.com]

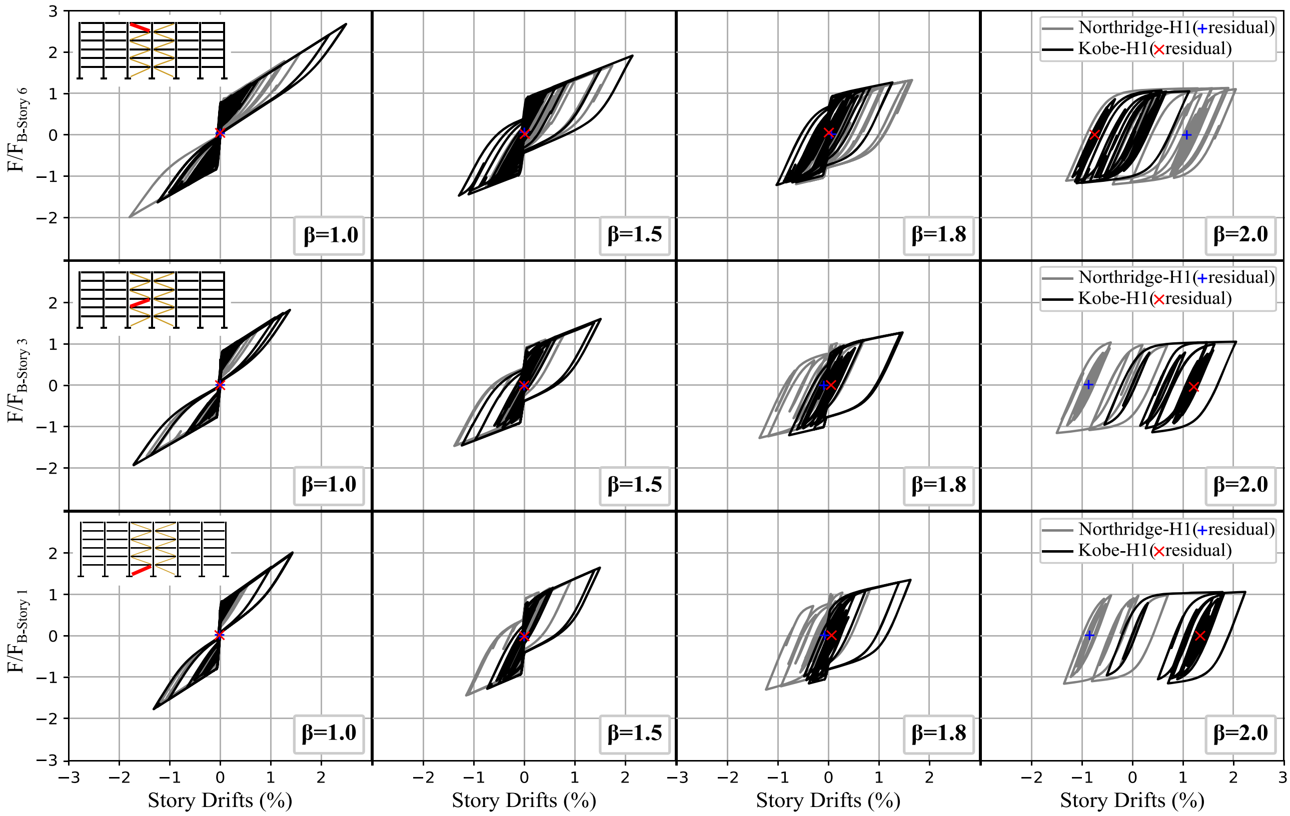

FIGURE 20 Response of braces for various stories under H1 component of RSN1116 Kobe and RSN960 Northridge-01 ground motions [Colour figure can be viewed at wileyonlinelibrary.com]

5.3 | Comparative study

This section describes a comparative study to evaluate seismic performances of PT-BRBs with newly proposed CFCCs and commonly used steel strands. In the example building, CFCCs are replaced with steel strands and seismic responses of two cases are compared. Behavior of the steel strand used is adopted from previous experimental studies.[22,31] A trilinear model that includes the posttensioning loss is considered (Figure 21A). Assumed behaviors of both CFCC and steel strand are illustrated on the same graph for a better comparison. Initial elastic modulus and yield strength of steel strand are E_{Str} = 196.5 GPa, $\sigma_{y\text{-}Str}$ = 1675.0 MPa, respectively. Yield strain ($\varepsilon_{y\text{-}Str}$) is fixed to 1% as per ASTM A1061/A1061M-16.[46] All properties of braces, including $F_{y\text{-}B}$ and α, until the yield point of steel strands are similar for corresponding β values. PT level is set equal to $0.25\sigma_{y\text{-}Str}$ (R_{PT} = 0.25) for steel strands. As shown in pushover curves of buildings incorporating PT-BRBs with steel strands (green lines) and CFCC (blue lines) in Figure 21B, building responses are similar until the steel strands have yielded in terms of α and β values. On the other hand, after the steel strands have yielded, postyield stiffness of the brace decreases when compared with the braces with CFCCs. In other words, postyield stiffness values are well maintained in the systems with CFCCs especially for lower β and higher α values. Such systems with higher postyield stiffness values improve SC features.

Figure 22A shows that average story drifts are slightly lesser in the case with CFCCs. This is mainly from the yielding of steel strands, especially in upper stories where average drifts exceed the yield limit for steel strands. Due loss of PT force and yielding of steel strands, average residual drifts are slightly larger than the case with CFCC (Figure 22B). As an example, brace hystereses at sixth floor under the H1 component of RSN1116 Kobe and RSN960 Northridge-01 ground motions are presented in Figure 22C. Note that other stories' braces experience various shapes of hystereses under these ground motions. As shown in Figure 22C, plastic deformation of steel strands has some side effects on the overall PT-BRB with steel strand performance. Firstly, it causes loss of all PT force on steel strands and a reduction in stiffness of the brace. Secondly, because of the plastic elongation, cables

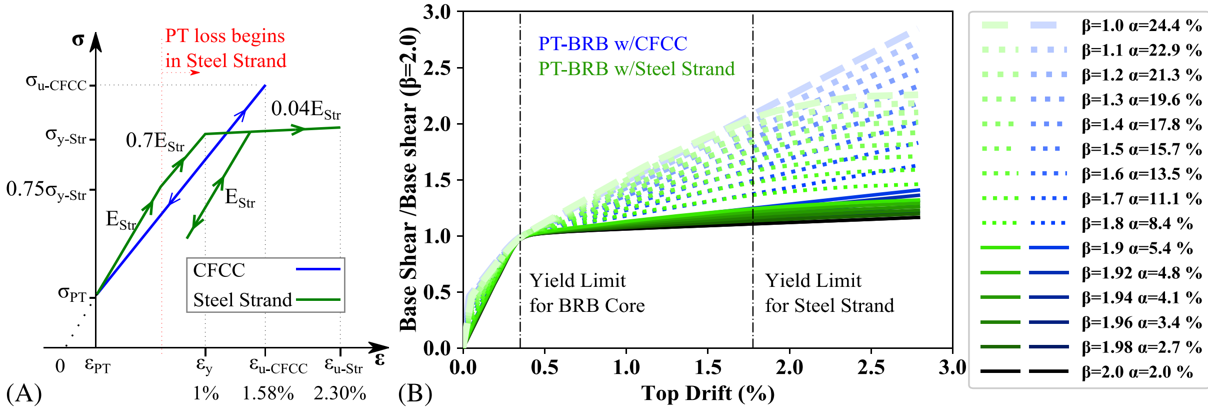

FIGURE 21 Numerical models and results A, material models for steel strand and carbon fiber composite cable (CFCC) B, comparative pushover curves for the example building incorporating posttensioned buckling restrained braces (PT-BRBs) with steel strands and CFCCs [Colour figure can be viewed at wileyonlinelibrary.com]

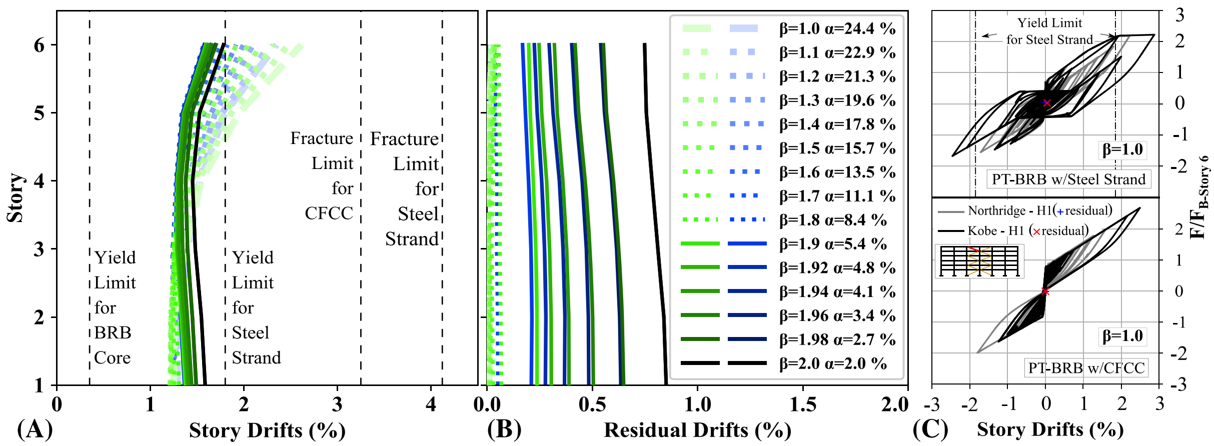

FIGURE 22 Seismic responses A, average story drifts, B, average residual drifts for the example building incorporating posttensioned buckling restrained braces (PT-BRBs) with PT-strands and carbon fiber composite cables (CFCCs), C, hysteretic responses of a brace at sixth story under H1 component of RSN1116 Kobe and RSN960 Northridge-01 ground motions [Colour figure can be viewed at wileyonlinelibrary.com]

are longer than the tubes in the plastic deformation phase of the strands, thus a distance (± plastic elongation) is necessary to activate steel strands. Additionally, hysteretic curves of PT-BRB with steel strands are similar to a conventional BRB because the only BRB is active in the region ± plastic elongations after steel strands have yielded.

Fracture limit of CFCCs ($\varepsilon_{u\text{-}CFCC}$) and steel strands ($\varepsilon_{u\text{-}CFCC}$) are larger than average story drifts. However, 0.16% of CFCCs and 0.11% of steel strands have fractured in all analyzed fully or partially SC braces. For both cases, top story cables have fractured under H2 component of RSN125 Friuli Italy-01. Note that the design might be optimized by changing $F_{y\text{-}B}$ distribution along the height of the example building. These results are intentionally given to show possible occurrence of cable failure under some ground motions; 12.2% of steel strands have yielded, in other words, have lost all PT forces. Even though side effect of yielding steel strands is limited on residual deformations, it may be required to replace these cables in a maintenance work following a major earthquake. PT-BRBs with CFCCs showed promise for use in new steel buildings as an alternative SC mechanism. Such evaluations are limited to the ground motions data and example building properties used in this paper. Also, results suggest that although both systems can be used with confidence, each of the systems considered have some advantages that may favor its implementation, depending on project-specific constraints.

6 | CONCLUSIONS

This study proposes an alternative type of BRB that can be used as an SC-BRB, a partially SC-BRB or a conventional BRB with controllable postyield stiffness ratio. Detailed specifications of the design steps, production process, and results from an experimental study that includes proof of concept cyclic component tests are provided. A numerical part is also added to explore the seismic effectiveness of a steel framed building incorporating PT-BRBs with several behavioral parameters already defined in the study. The following results are obtained from experimental and numerical analyses:

1. From cyclic (not fully reversed) coupon test results of the CFCC members, the anchorage system with HEM exhibited sufficient force capacity to transfer forces to the end plates. Slippage or placing of the anchorage system causes permanent deformations, and thus anchorage system response is highly effective when CFCCs are used as an external posttensioned element on the brace. The behavior of CFCC becomes linear after a certain level of force is applied. Hence, a PT path is recommended for obtaining a linear response and proving strength. Coupon test results indicated that CFCCs exhibited very stable behavior with limited loss in posttension.
2. Reversed cyclic component tests reveal that the developed PT-BRBs exhibit stable hystereses even after the core or cables are fractured. The braces achieved 2% story drift as per the AISC protocol for qualification of BRBs. Force transfer of the SC mechanisms did not occur instantly due length tolerance, rotation, and difference in stiffness although ±2 mm was sufficient to transfer all the forces. Maximum compression strength adjustment factor ($\beta_{co\text{-}B}$) and minimum cumulative plastic deformation of the braces before fracture (CPD_B) agreed with the conventional BRB requirements as provided in the AISC Seismic Provisions.
3. Results from the numerical model proposed for the PT-BRB component were in good agreement with the experimental data. Numerical studies conducted on steel frames with pinned connections and braced with PT-BRBs indicate that requirements of the current codes can be achieved in the selected building when PT-BRBs are used. Nonlinear time history analyses suggest that increases in PT force and postyield stiffness of the braces decrease residual drifts. However, capacity-based design forces significantly affect section sizes of other members. Given the limited scope of the study, the use of PT-BRBs with $\beta = 1.8$ can also be termed as the "partially self-centering" BRB provided low peak drift ratios and negligible residual drifts for the ground motion data are considered in the study. Individual ground motion analysis results show that increases in PT force provide more centered behavior and this can also reduce also peak drifts even energy dissipation potential is lesser than a bilinear hysteresis.
4. As CFCCs have limited loss of posttensioning force under cyclic loading, recentering behavior is more stable than steel strands. When compared with CFCCs, steel strands possess better ductility capacities due to their higher elongation capacity. Comparative numerical analyses conducted for the selected systems incorporating PT-BRBs with CFCCs and steel strands reveal that average peak and residual drifts are slightly lesser in the case with CFCCs.

ACKNOWLEDGEMENTS

The first author thanks the TUBITAK 2214-A International Doctoral Research Fellowship Programme for financial support during his research at Tokyo Institute of Technology (TIT). We acknowledge support from Mr. Kenichi Hayashi of Nippon Steel Engineering Co. Ltd. for the production of braces tested in this study.

ORCID

Kurtulus Atasever https://orcid.org/0000-0002-8100-0699
Shogo Inanaga https://orcid.org/0000-0002-8971-1479
Toru Takeuchi https://orcid.org/0000-0001-7430-4734
Yuki Terazawa https://orcid.org/0000-0003-4808-1885
Oguz C. Celik https://orcid.org/0000-0001-9448-2562

REFERENCES

1. Uang C, Bruneau M. State-of-the-art review on seismic design of steel structures. *J Struct Eng*. 2018;144(4):03118002-1-03118002-24. https://doi.org/10.1061/(ASCE)ST.1943-541X.0001973
2. Miranda E. Lessons learned from the 2010 Haiti earthquake for performance-based design. *Geotech Geol Earthquake Eng*. 2014;32:117-127. https://doi.org/10.1007/978-94-017-8875-5_9

3. Buchanan AH, Honey BG. Energy and carbon dioxide implications of building construction. *Energ Buildings*. 1994;20(3):205-217. https://doi.org/10.1016/0378-7788(94)90024-8
4. Macrae GA, Kawashima K. Post-earthquake residual displacements of bilinear oscillators. *Earthq Eng Struct Dyn*. 1997;26(7):701-716. https://doi.org/10.1002/(SICI)1096-9845(199707)26:7<701::AID-EQE671>3.0.CO;2-I
5. Connor JJ, Wada A, Iwata M, Huang YH. Damage-controlled structures. I: preliminary design methodology for seismically active regions. *J Struct Eng*. 1997;123(4):423-430.
6. Priestley MJN, Sritharan S, Conley JR, Stefano PS. Preliminary results and conclusions from the PRESSS five-story precast concrete test building. *PCI J*. 1999;44(6):42-67. https://doi.org/10.15554/pcij.11011999.42.67
7. Christopoulos C, Filiatrault A, Uang CM, Folz B. Posttensioned energy dissipating connections for moment-resisting steel frames. *J Struct Eng*. 2002;128(9):1111-1120. https://doi.org/10.1061/(ASCE)0733-9445(2002)128:9(1111)
8. Ma X, Deierlein G, Eatherton M, et al. Large-scale shaking table test of steel braced frame with controlled rocking and energy dissipating fuses. *9th US National and 10th Canadian Conference on Earthquake Engineering 2010, Including Papers from the 4th International Tsunami Symposium*, vol. 3, 2010. https://scholar.google.com/scholar?q=Large%E2%80%90scale+shaking+table+test+of+steel+braced+frame+with+controlled+rocking+and+energy+dissipating+fuses&hl=tr&as_sdt=0,5
9. Nims DK, Richter PJ, Bachman RE. The use of the energy dissipating restraint for seismic hazard mitigation. *Earthq Spectra*. 1993;9(3):467-489. https://doi.org/10.1193/1.1585725
10. Christopoulos C, Filiatrault A, Folz B. Seismic response of self-centring hysteretic SDOF systems. *Earthq Eng Struct Dyn*. 2002;31(5):1131-1150. https://doi.org/10.1002/eqe.152
11. Zhu S, Zhang Y. Seismic behaviour of self-centring braced frame buildings with reusable hysteretic damping brace. *Earthq Eng Struct Dyn*. 2007;36(10):1329-1346. https://doi.org/10.1002/eqe.683
12. Christopoulos C, Tremblay R, Kim HJ, Lacerte M. Self-centering energy dissipative bracing system for the seismic resistance of structures: development and validation. *J Struct Eng*. 2008;134(1):96-107. https://doi.org/10.1061/(ASCE)0733-9445(2008)134:1(96)
13. Erochko J, Christopoulos C, Tremblay R. Design, testing, and detailed component modeling of a high-capacity self-centering energy-dissipative brace. *J Struct Eng*. 2015;141(8):04014193-1-04014193-12. https://doi.org/10.1061/(ASCE)ST.1943-541X.0001166
14. Chou CC, Chen YC. Development of steel dual-core self-centering braces: quasi-static cyclic tests and finite element analyses. *Earthq Spectra*. 2015;31(1):247-272. https://doi.org/10.1193/082712EQS272M
15. Miller DJ, Fahnestock LA, Eatherton MR. Development and experimental validation of a nickel-titanium shape memory alloy self-centering buckling-restrained brace. *Eng Struct*. 2012;40:288-298. https://doi.org/10.1016/j.engstruct.2012.02.037
16. Fujimoto M, Wada A, Saeki E, Watanabe A, Hitomi Y. A study on the unbounded brace encased in buckling-restraining concrete and steel tube. *J Struct Eng*. 1988;34:249-258.
17. Sabelli R, Mahin S, Chang C. Seismic demands on steel braced frame buildings with buckling-restrained braces. *Eng Struct*. 2003;25(5):655-666. https://doi.org/10.1016/S0141-0296(02)00175-X
18. Erochko J, Christopoulos C, Tremblay R, Choi H. Residual drift response of SMRFs and BRB frames in steel buildings designed according to ASCE 7-05. *J Struct Eng*. 2011;137(5):589-599. https://doi.org/10.1061/(ASCE)ST.1943-541X.0000296
19. Zhou Z, Xie Q, Lei XC, He XT, Meng SP. Experimental investigation of the hysteretic performance of dual-tube self-Centering buckling-restrained braces with composite tendons. *J Compos Constr*. 2015;19(6):1-13. https://doi.org/10.1061/(ASCE)CC.1943-5614.0000565
20. Eatherton MR, Hajjar JF. Residual drifts of self-centering systems including effects of ambient building resistance. *Earthq Spectra*. 2011;27(3):719-744. https://doi.org/10.1193/1.3605318
21. Erochko J. *Improvements to the Design and Use of Post-Tensioned Self-Centering Energy-Dissipative (SCED) Braces*. Toronto, Ontario: Doctoral Thesis, University of Toronto; 2013.
22. Maurya A. *Experimental and computational investigation of a self-centering beam moment frame (SCB-MF)*. Blacksburg, VA: Doctoral Thesis, Virginia Tech; 2016.
23. Takeuchi T, Wada A, Matsui R, et al. Buckling-Restrained Braces and Applications, Chapter 1: Composition and history of Buckling-restrained braces. In: *Buckling-Restrained Braces and Applications*. Tokyo, Japan: The Japan Society of Seismic Isolation (JSSI); 2017.
24. American Society of Civil Engineers (ASCE). Minimum Design Loads and Associated Criteria for Buildings and Other Structures, ASCE/SEI 7-16. Reston, Virginia; 2017. https://doi.org/10.1061/9780784414248.
25. Kersting RA, Fahnestock LA, López WA. Seismic design of steel buckling-restrained braced frames a guide for practicing engineers about the review panel. *NEHRP Seismic Design Technical Brief* (11).
26. Santoh N. CFCC (carbon fiber composite cable). In: *Fiber-Reinforced-Plastic (FRP) Reinforcement for Concrete Structures*. Amsterdam: Elsevier; 1993.
27. Kimura H, Kawata K, Itabashi M. Analysis of tensile behavior of cfrp strand cables with various structures. *Adv Compos Mater*. 1996;6(1):19-32. https://doi.org/10.1163/156855196X00176
28. Kimura H, Itabashi M, Kawata K. Mechanical characterization of unidirectional CFRP thin strip and CFRP cables under quasi-static and dynamic tension. *Advanced Composite Materials*. 2001;10(2-3):177-187. https://doi.org/10.1163/156855101753396654
29. ASTM-D7205/D7205M-06. ASTM-D7205 standard test method for tensile properties of fiber reinforced polymer matrix composite bars. *Standard Test Method for Tensile Properties of Fiber Reinforced Polymer Matrix* 2011; i (Reapproved 2011): 1-13. https://doi.org/10.1520/D7205.
30. Khin M. *Fundamental Study On Bond and Anchorage of Continuous Fiber Reinforcing Materials*. Japan: Kyushu Institute of Technology; 2001.

31. Bruce TL, Eatherton MR. Behavior of post-tensioning strand systems subjected to inelastic cyclic loading. *J Struct Eng (United States)*. 2016;142(10):04016067-1-04016067-13. https://doi.org/10.1061/(ASCE)ST.1943-541X.0001503
32. Applied Technology Council. FEMA 461/interim testing protocols for determining the seismic performance characteristics of structural and nonstructural components; 2007.
33. American Institute of Steel Construction. ANSI/AISC 341-16, seismic provisions for structural steel buildings. *Seismic Provisions for Structural Steel Buildings*; 2016. DOI: 111.
34. Zhu M, McKenna F, Scott MH. OpenSeesPy: Python library for the OpenSees finite element framework. *SoftwareX*. 2018;7:6-11. https://doi.org/10.1016/j.softx.2017.10.009
35. Eatherton MR, Fahnestock LA, Miller DJ. Computational study of self-centering buckling-restrained braced frame seismic performance. *Earthq Eng Struct Dyn*. 2014;43(13):1897-1914. https://doi.org/10.1002/eqe.2428
36. Filippou FC, Povpov EP, Bertero VV. Effects of bond deterioration on hysteretic behavior of reinforced concrete joints. Earthquake Engineering Research Center; 1983.
37. Kolozvari K, Orakcal K, Wallace JW. Modeling of Cyclic Shear-Flexure Interaction in Reinforced Concrete Structural Walls. I: Theory. *Journal of Structural Engineering*. 2015;141(5):04014135-1-04014135-10. https://doi.org/10.1061/(asce)st.1943-541x.0001059
38. Applied Technology Council & USFEMA. FEMA P695/quantification of building seismic performance factors. US Department of Homeland Security, FEMA; 2009.
39. Charney FA. Unintended consequences of modeling damping in structures. *J Struct Eng*. 2008;134(4):581-592. https://doi.org/10.1061/(ASCE)0733-9445(2008)134:4(581)
40. Bosco M, Marino EM. Design method and behavior factor for steel frames with buckling restrained braces. *Earthq Eng Struct Dyn*. 2013;42(8):1243-1263. https://doi.org/10.1002/eqe.2269
41. Tremblay R, Dehghani M, Fahnestock L, et al. Comparison of seismic design provisions for buckling restrained braced frames in Canada, United States, Chile, and New Zealand. *Structure*. 2016;8:183-196. https://doi.org/10.1016/j.istruc.2016.06.004
42. Pacific Earthquake Engineering Research Center. Technical report for the PEER ground motion database web application; 2010(November).
43. Ancheta TD, Darragh RB, Stewart JP, et al. NGA-West2 Database. *Earthquake Spectra*. 2014;30(3):989-1005. https://doi.org/10.1193/070913eqs197m
44. Wu AC, Lin PC, Tsai KC. High-mode buckling responses of buckling-restrained brace core plates. *Earthq Eng Struct Dyn*. 2014;43(3):375-393. https://doi.org/10.1002/eqe.2349
45. McCormick J, Aburano H, Ikenaga M, Nakashima M. Permissible residual deformation levels for building structures considering both safety and human elements. *The 14th World Conference on Earthquake Engineering*; 2008:8.
46. A1061/A1061M-16 A. Standard test methods for testing multi-wire steel prestressing strand 1; 2018: 3–6. DOI: 10.1520/A1061.

How to cite this article: Atasever K, Inanaga S, Takeuchi T, Terazawa Y, Celik OC. Experimental and numerical studies on buckling restrained braces with posttensioned carbon fiber composite cables. *Earthquake Engng Struct Dyn*. 2020;1–22. https://doi.org/10.1002/eqe.3321